Symmetry restoring bifurcations and quasiperiodic chaos induced by a new intermittency in a vibro-impact system

Yuan Yue, Pengcheng Miao, Jianhua Xie, and Grebogi Celso

Citation: Chaos **26**, 113121 (2016); doi: 10.1063/1.4968552
View online: http://dx.doi.org/10.1063/1.4968552
View Table of Contents: http://scitation.aip.org/content/aip/journal/chaos/26/11?ver=pdfcov
Published by the AIP Publishing

Symmetry restoring bifurcations and quasiperiodic chaos induced by a new intermittency in a vibro-impact system

Yuan Yue,[1] Pengcheng Miao,[1] Jianhua Xie,[1] and Grebogi Celso[2]
[1]*Applied Mechanics and Structure Safety Key Laboratory of Sichuan Province, School of Mechanics and Engineering, Southwest Jiaotong University, Chengdu 610031, China*
[2]*Institute for Complex Systems and Mathematical Biology King's College, University of Aberdeen, Aberdeen AB24 3UE, United Kingdom*

(Received 2 June 2016; accepted 9 November 2016; published online 29 November 2016)

Quasiperiodic chaos (QC), which is a combination of quasiperiodic sets and a chaotic set, is uncovered in the six dimensional Poincaré map of a symmetric three-degree of freedom vibro-impact system. Accompanied by symmetry restoring bifurcation, this QC is the consequence of a novel intermittency that occurs between two conjugate quasiperiodic sets and a chaotic set. The six dimensional Poincaré map **P** is the 2-fold composition of another virtual implicit map **Q**, yielding the symmetry of the system. Map **Q** can capture two conjugate attractors, which is at the core of the dynamics of the vibro-impact system. Three types of symmetry restoring bifurcations are analyzed in detail. First, if two conjugate chaotic attractors join together, the chaos-chaos intermittency induced by attractor-merging crisis takes place. Second, if two conjugate quasiperiodic sets are suddenly embedded in a chaotic one, QC is induced by a new intermittency between the three attractors. Third, if two conjugate quasiperiodic attractors connect with each other directly, they merge to form a single symmetric quasiperiodic one. For the second case, the new intermittency is caused by the collision of two conjugate quasiperiodic attractors with an unstable symmetric limit set. As the iteration number is increased, the largest finite-time Lyapunov exponent of the QC does not converge to a constant, but fluctuates in the positive region. *Published by AIP Publishing.*
[http://dx.doi.org/10.1063/1.4968552]

Crisis and intermittency, existing commonly in various dynamical systems, have been important issues in nonlinear dynamical systems. However, nearly all previous studies on crisis and intermittency have concentrated on low-dimensional dynamical systems which have not quasi-periodic attractors (i.e., torus motion in original phase space). In this paper, we consider a three-degree of freedom vibro-impact system with symmetry, and obtain a six-dimensional virtual implicit map to describe its dynamics. A novel attractor—the quasiperiodic chaos attractor (QC), which is a combination of quasiperiodic sets and a chaotic set, is uncovered. We show that the QC is induced by a new intermittency among two conjugate quasiperiodic sets and a chaotic set. Accompanied by a symmetry restoring bifurcation, this intermittency is induced by a new crisis occurring in high-dimensional symmetric dynamical systems.

I. INTRODUCTION

Intermittency historically refers to the state in which the laminar flow is interrupted by turbulent outbreaks or bursts at irregular intervals in fluid mechanics. It is known that intermittencies also exist in low-dimensional dynamical systems, and have been classified as type I, type II, and type III intermittency[1] which are related to cyclic-fold bifurcation, subcritical Hopf bifurcation and subcritical period-doubling bifurcation, respectively. However, there is another type of intermittency, named crisis-induced intermittency, which is qualitatively different in the mechanism from the above three intermittencies. The term crisis[2] was first used by Grebogi, Ott, and Yorke to describe the phenomenon of the collision of the unstable orbit with another attractor. Three types of crises are distinguished, according to the nature of the discontinuity induced in the chaotic attractor. They are boundary crisis, interior crisis and attractor-merging crisis.[3] For the interior crisis and attractor-merging crisis, the term *crisis-induced intermittency*[4] is used to describe the characteristic temporal behavior which occurs after the crisis. In this case, in contrast to type I, type II, and type III, the temporal evolution is characterized by the irregular switching among different kinds of chaotic dynamics. There is another class of bifurcations, called symmetry breaking,[5] symmetry increasing via collision[6] and symmetry increasing via explosion,[7] are all the result of a collision between conjugate attractors (i.e., attractors that related to each other by the symmetry) and a symmetric limit set. Besides, the term *symmetry restoring* bifurcation[8] is used to describe the transition in which a non-symmetric limit set becomes symmetric at the critical point of this collision as a system parameter changes. Since the unstable symmetric limit set plays the key role in the symmetry restoring bifurcation, it is important to determine the unstable periodic orbit[9] or unstable chaotic set (i.e., chaotic saddle in two dimensional cases).[10] Nearly all previous studies on symmetry restoring bifurcation, crisis, and intermittency have aimed at low-dimensional dynamical systems that have no quasiperiodic attractor. However, quasiperiodic attractors, which take place in high-dimensional dynamical

systems, may bring something new to crisis, intermittency, and symmetry by restoring bifurcations in dynamical systems. In this paper, we analyze three types of symmetry restoring bifurcations in a three degree of freedom vibro-impact system. We show that a quasiperiodic attractor (i.e., motion on 2-torus in the phase space) has two types of symmetry restoring bifurcations. Moreover, a quasiperiodic chaos (QC) induced by a new intermittency among three sets is identified. Accompanied by a symmetry restoring bifurcation, this intermittency is caused by the collision between two conjugate quasiperiodic sets and an unstable symmetric limit set.

Vibro-impact systems, highly relevant to applications, are strongly nonlinear, exhibiting abundant dynamical behaviors and offering a good platform for the study of nonlinear dynamics. Some selected applications of vibro-impact dynamics are vibratory hammers, a bouncing ball on an oscillating barrier, mass-spring-dashpot systems with rigid constraints, dynamical action between wheel and rail, pipes conveying fluids with end-restraints, nuclear reactors, and heat exchangers. Till now, the studies on vibro-impact system include the existence of periodic motion and its stability, bifurcation and chaotic behaviour in the single degree of freedom vibro-impact systems,[11,12] codimension two and three bifurcations in the multi-degree of freedom vibro-impact systems,[13–16] and non-typical bifurcations induced by grazing.[17,18] For some other noteworthy studies on the dynamics of vibro-impact systems in recent years see Refs. 19–22. However, for the multi-degree of freedom vibro-impact system, studies on the symmetry restoring bifurcation of quasiperiodic attractor and intermittency have not been reported up to now.

In this paper, we consider a three-degree-of-freedom vibro-impact system with symmetry which has been studied in Refs. 15, 19, and 20, and analyze three types of symmetry restoring bifurcations. It is shown that a new mixed attractor, which is a combination of quasiperiodic sets and a chaotic set, yields a new intermittency on the attractors. The paper is organised as follows. In Section II, the mechanical model is presented, the six dimensional virtual implicit Poincaré map **Q** is derived, and the Lyapunov exponents computational results are given. In Section III, the symmetric limit set is defined, and a distance between two conjugate attractors and the unstable symmetric fixed point is introduced. In Section IV, through numerical simulations, three types of symmetry restoring bifurcations and a special mixed attractor caused by the new intermittency are investigated. Conclusions are given in Section V.

II. MECHANICAL MODEL, POINCARÉ MAP, AND LYAPUNOV EXPONENTS

A three-degree-of-freedom system with symmetric two-sided rigid constraints[15,19,20] is shown in Fig. 1. The system has three masses M_1, M_2, and M_3. M_2 is connected to a rigid plane via a linear spring K_2 and a linear viscous dashpot C_2. M_1 and M_3 are connected to M_2 via linear springs K_1 and K_3, and linear viscous dashpots C_1 and C_3, respectively. The excitation on mass M_i $(i = 1, 2, 3)$ is harmonic with amplitude P_i. For small forcing amplitude the system undergoes

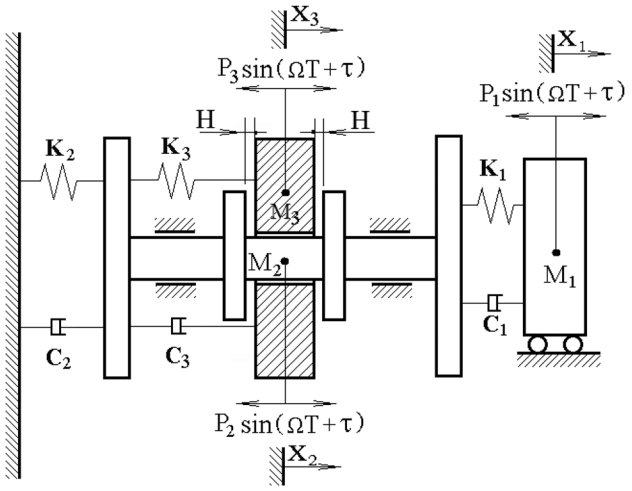

FIG. 1. Three degree of freedom vibro-impact system with symmetry.

simple oscillations and behaves as a linear system. However, as the amplitude is increased, M_3 begins to collide with two stops of M_2, and the system becomes strongly nonlinear. The impact is described by a coefficient of restitution r. It is assumed that the duration of impact is negligible compared to the period of the force. C_1, C_2, and C_3 are assumed as proportional damping.

Between any two consecutive impacts, the non-dimensional differential equation of motion is given by[15,19]

$$\mathbf{U}_m\ddot{x} + 2\zeta\mathbf{U}_c\dot{x} + \mathbf{U}_k x = \mathbf{U}_f f\sin(\omega t + \tau), \tag{1}$$

where $x = [x_1, x_2, x_3]^{\mathbf{T}}$, $\mathbf{U}_m = diag[u_{m_1}, u_{m_2}, u_{m_3}]$, $\mathbf{U}_f = diag[u_{f_1}, u_{f_2}, u_{f_3}]$, $\mathbf{U}_c = \begin{bmatrix} u_{c_1} & -u_{c_1} & 0 \\ -u_{c_1} & u_{c_1}+u_{c_2}+u_{c_3} & -u_{c_3} \\ 0 & -u_{c_3} & u_{c_3} \end{bmatrix}$, $\mathbf{U}_k = \begin{bmatrix} u_{k_1} & -u_{k_1} & 0 \\ -u_{k_1} & u_{k_1}+u_{k_2}+u_{k_3} & -u_{k_3} \\ 0 & -u_{k_3} & u_{k_3} \end{bmatrix}$. The non-dimensional variables and parameters are $t = T\sqrt{\frac{K_1}{M_1}}$, $\zeta = \frac{C_1}{2\sqrt{K_1 M_1}}$, $\omega = \Omega\sqrt{\frac{M_1}{K_1}}$, $f = \frac{P_1}{P_0}$, $u_{m_i} = \frac{M_i}{M_1}$, $u_{k_i} = \frac{K_i}{K_1}$, $u_{c_i} = \frac{C_i}{C_1}$, $u_{f_i} = \frac{P_i}{P_1}$, $x_i = \frac{X_i K_1}{P_0}$, where $P_0 = \sum_{i=1}^{3}|P_i|$, $i = 1, 2, 3$.

As M_3 collides with the left and the right stops of M_2, the non-dimensional displacements of the two masses satisfy $|x_2 - x_3| \equiv h$, where $h = \frac{K_1 H}{P_0}$. Newton's impact model is used for the process of impact. The velocity of M_i at time t is denoted by $y_i(t) = \dot{x}_i(t)$. Let $y_{i-} = \dot{x}_{i-}$, $y_{i+} = \dot{x}_{i+}$ be the non-dimensional velocities of M_i before and after impact, respectively. After each impact, the velocities of M_2 and M_3 change as follows according to the impact law and the momentum conservation rule:

$$y_{2+} = \delta_{11}y_{2-} + \delta_{12}y_{3-}, \quad y_{3+} = \delta_{21}y_{2-} + \delta_{22}y_{3-}, \tag{2}$$

where $\delta_{11} = \frac{1-r\kappa}{1+\kappa}$, $\delta_{12} = \frac{(1+r)\kappa}{1+\kappa}$, $\delta_{21} = \frac{1+r}{1+\kappa}$, $\delta_{22} = \frac{-r+\kappa}{1+\kappa}$, and $\kappa = \frac{u_{m3}}{u_{m2}}$.

The eigenfrequencies of Eq. (1) can be solved as ω_1, ω_2, and ω_3. Taking $\boldsymbol{\psi}$ as the canonical model matrix, and making the change of variable $[x_1, x_2, x_3]^{\mathbf{T}} = \boldsymbol{\psi}\xi$, Eq. (1) becomes

$$\mathbf{I}\ddot{\xi} + \mathbf{C}\dot{\xi} + \mathbf{\Lambda}\xi = \boldsymbol{\psi}^{\mathbf{T}}\mathbf{U}_f f\sin(\omega t + \tau), \tag{3}$$

where $\mathbf{\Lambda} = diag[\omega_1^2, \omega_2^2, \omega_3^2]$, $\mathbf{C} = 2\zeta\mathbf{\Lambda}$. Let ψ_{kj} be the element of $\boldsymbol{\psi}$, the general solution of Eq. (1) is given by

$$x_i(t) = \sum_{j=1}^{3}\psi_{ij}\{e^{-\eta_j t}[a_j\cos(\omega_{dj}t) + b_j\sin(\omega_{dj}t)] + A_j\sin(\omega t + \tau) + B_j\cos(\omega t + \tau)\}, \tag{4-1}$$

$$y_i(t) = \sum_{j=1}^{3}\psi_{ij}\{e^{-\eta_j t}[(-\eta_j a_j + \omega_{dj}b_j)\cos(\omega_{dj}t) + (-\eta_j b_j - \omega_{dj}a_j)\sin(\omega_{dj}t)] + A_j\omega\cos(\omega t + \tau) - B_j\omega\sin(\omega t + \tau)\}, \tag{4-2}$$

where $\eta_j = \zeta\omega_j^2$, $\omega_{dj} = \sqrt{\omega_j^2 - \eta_j^2}$, and a_j and b_j are integration constants determined by initial conditions, A_j and B_j are amplitude constants.

The Poincaré section is chosen after the impact at the left stop (i.e., $x_2 - x_3 \equiv h$). The Poincaré map $\mathbf{P}$ is a composition of the following four sub-maps: (a) $\mathbf{P}_1$: The map from the instant after impacting at the left stop to the instant before impacting at the right stop, where the state coordinates are determined by Eq. (4); (b) $\mathbf{P}_2$: The map of impacting at the right stop, where only the coordinates y_2 and y_3 change according to Eq. (2); (c) $\mathbf{P}_3$: The map from the instant after impacting at the right stop to the instant before impacting at the left stop, where the state coordinates are determined by Eq. (4); (d) $\mathbf{P}_4$: The map of impacting at the left stop, where only coordinates y_2 and y_3 change according to Eq. (2). Hence, the Poincaré map can be expressed as $\mathbf{P} = \mathbf{P}_4 \circ \mathbf{P}_3 \circ \mathbf{P}_2 \circ \mathbf{P}_1$.

Equation (1) can be rewritten as $\dot{\mathbf{X}} = \mathbf{F}(\mathbf{X}, t)$, where $\mathbf{X} = (x_1, y_1, x_2, y_2, x_3, y_3)^{\mathrm{T}}$. Based on the fact that $\mathbf{F}(\mathbf{X}, t + \frac{2\pi}{\omega}) = \mathbf{F}(\mathbf{X}, t)$ and $\mathbf{F}(-\mathbf{X}, t + \frac{\pi}{\omega}) = -\mathbf{F}(\mathbf{X}, t)$, it has been proved that[15]

$$\mathbf{P} = \mathbf{Q}^2. \tag{5}$$

That is, the Poincaré map $\mathbf{P}$ is the 2-fold composition of another map $\mathbf{Q}$, where

$$\mathbf{Q} = \Re^{\pm 1} \circ \mathbf{Q}_1, \tag{6}$$

where $\Re$ is the transformation

$$\Re : (x_1, y_1, x_2, y_2, x_3, y_3, t) \mapsto \left(-x_1, -y_1, -x_2, -y_2, -x_3, -y_3, t + \frac{\pi}{\omega}\right), \tag{7}$$

and $\mathbf{Q}_1 = \mathbf{P}_2 \circ \mathbf{P}_1$. In Ref. 15, it has been proved that Eq. (5) stands in the case of $\mathbf{Q} = \Re \circ \mathbf{Q}_1$. In fact, based on Eq. (7), $\Re^2 = \Re^{-2} = \mathbf{I}$ is a unit transformation. Hence $\mathbf{Q} = \Re \circ \mathbf{Q}_1 = \Re^{-2} \circ \Re \circ \mathbf{Q}_1 = \Re^{-1} \circ \mathbf{Q}_1$. Therefore, Eq. (5) stands for both $\mathbf{Q} = \Re^{+1} \circ \mathbf{Q}_1$ and $\mathbf{Q} = \Re^{-1} \circ \mathbf{Q}_1$.

The map $\mathbf{Q}$ in Eq. (6) can be expressed as

$$\mathbf{Q} : \mathbf{R}^6 \to \mathbf{R}^6 :$$

$$x_1(n+1) = -\sum_{j=1}^{3}\psi_{1j}\{e^{-\eta_j t}[a_j\cos(\omega_{dj}t) + b_j\sin(\omega_{dj}t)] + A_j\sin(\omega t + \tau(n)) + B_j\cos(\omega t + \tau(n))\}, \tag{8-1}$$

$$y_1(n+1) = -\sum_{j=1}^{3}\psi_{1j}\{e^{-\eta_j t}[(-\eta_j a_j + \omega_{dj}b_j)\cos(\omega_{dj}t) + (-\eta_j b_j - \omega_{dj}a_j)\sin(\omega_{dj}t)] + A_j\omega\cos(\omega t + \tau(n)) - B_j\omega\sin(\omega t + \tau(n))\}, \tag{8-2}$$

$$x_2(n+1) = -\sum_{j=1}^{3}\psi_{2j}\{e^{-\eta_j t}[a_j\cos(\omega_{dj}t) + b_j\sin(\omega_{dj}t)] + A_j\sin(\omega t + \tau(n)) + B_j\cos(\omega t + \tau(n))\}, \tag{8-3}$$

$$y_2(n+1) = -\delta_{11}\sum_{j=1}^{3}\psi_{2j}\{e^{-\eta_j t}[(-\eta_j a_j + \omega_{dj}b_j)\cos(\omega_{dj}t) + (-\eta_j b_j - \omega_{dj}a_j)\sin(\omega_{dj}t)] + A_j\omega\cos(\omega t + \tau(n)) - B_j\omega\sin(\omega t + \tau(n))\} - \delta_{12}\sum_{j=1}^{3}\psi_{3j}\{e^{-\eta_j t}[(-\eta_j a_j + \omega_{dj}b_j)\cos(\omega_{dj}t) + (-\eta_j b_j - \omega_{dj}a_j)\sin(\omega_{dj}t)] + A_j\omega\cos(\omega t + \tau(n)) - B_j\omega\sin(\omega t + \tau(n))\}, \tag{8-4}$$

$$y_3(n+1) = -\delta_{21}\sum_{j=1}^{3}\psi_{2j}\{e^{-\eta_j t}[(-\eta_j a_j + \omega_{dj}b_j)\cos(\omega_{dj}t) + (-\eta_j b_j - \omega_{dj}a_j)\sin(\omega_{dj}t)] + A_j\omega\cos(\omega t + \tau(n)) - B_j\omega\sin(\omega t + \tau(n))\} - \delta_{22}\sum_{j=1}^{3}\psi_{3j}\{e^{-\eta_j t}[(-\eta_j a_j + \omega_{dj}b_j)\cos(\omega_{dj}t) + (-\eta_j b_j - \omega_{dj}a_j)\sin(\omega_{dj}t)] + A_j\omega\cos(\omega t + \tau(n)) - B_j\omega\sin(\omega t + \tau(n))\}, \tag{8-5}$$

$$\tau(n+1) = \tau(n) + \omega t + \pi(\mathrm{mod}(2\pi)), \tag{8-6}$$

where integration constants a_i and b_i $(i = 1, 2, 3)$ can be expressed as the function of the initial conditions

$$a_i(x_1(n), x_2(n), \tau(n)) = \alpha_{1i}x_1(n) + \alpha_{2i}x_2(n) + \alpha_{3i}\sin\tau(n) + \alpha_{4i}\cos\tau(n) + \alpha_{5i}, \tag{9-1}$$

$$b_i(x_1(n), y_1(n), x_2(n), y_2(n), y_3(n), \tau(n)) = \beta_{1i}x_1(n) + \beta_{2i}x_2(n) + \beta_{3i}y_1(n) + \beta_{4i}y_2(n) + \beta_{5i}y_3(n) + \beta_{6i}\sin\tau(n) + \beta_{7i}\cos\tau(n) + \beta_{8i}, \tag{9-2}$$

where α_{ji} $(j = 1, \ldots, 5)$ and β_{ki} $(k = 1, \ldots, 8)$ are constants determined by system parameters, n and n + 1 denote the

iteration number of map **Q**. It should be noted that since $x_2 - x_3 \equiv h$ in the Poincaré section, $x_3(n+1)$ can be determined by $x_2(n+1)$, hence it does not appear in Eq. (8). The time t in Eq. (8) is the unique solution of the following equation due to $x_2 - x_3 - h \equiv 0$ for the Poincaré map **P**:

$$\begin{aligned} G &= x_2(n+1) - x_3(n+1) - h \\ &= \sum_{j=1}^{3} \psi_{2j}\{e^{-\eta_j t}[a_j \cos(\omega_{dj} t) + b_j \sin(\omega_{dj} t)] \\ &\quad + A_j \sin(\omega t + \tau(n)) + B_j \cos(\omega t + \tau(n))\} \\ &\quad - \sum_{j=1}^{3} \psi_{3j}\{e^{-\eta_j t}[a_j \cos(\omega_{dj} t) + b_j \sin(\omega_{dj} t)] \\ &\quad + A_j \sin(\omega t + \tau(n)) + B_j \cos(\omega t + \tau(n))\} - h = 0. \end{aligned} \tag{10}$$

The value of t has no analytic expression, implying that $\mathbf{Q}_1$, **Q**, and **P** are all implicit maps.

As shown in Ref. 15, the fixed point of map **P** (i.e., the solution of $\mathbf{X}^* = \mathbf{P}(\mathbf{X}^*)$) corresponds to the associated periodic motion of the system, and the fixed point of map **Q** (i.e., the solution of $\mathbf{X}^* = \mathbf{Q}(\mathbf{X}^*)$) corresponds to the associated symmetric period *n*–2 motion of the system. According to Eq. (6), $\mathbf{X}^* = \mathbf{Q}(\mathbf{X}^*)$ means $\Re\mathbf{X}^* = \mathbf{Q}_1(\mathbf{X}^*)$, which implies that after M_3 impacts the right and the left stops, the associated state coordinates of the system are equal in absolute value and opposite in direction. At the same time, $\mathbf{X}^* = \mathbf{Q}(\mathbf{X}^*)$ also implies $\mathbf{X}^* = \mathbf{P}(\mathbf{X}^*)$ since $\mathbf{P} = \mathbf{Q}^2$, then $\mathbf{X}^*$ is called a *symmetric* fixed point of the Poincaré map **P**. For both stable and unstable cases, the symmetric fixed point $\mathbf{X}^*$ can be determined analytically by $\mathbf{X}^* = \mathbf{Q}(\mathbf{X}^*)$, see Ref. 15 for details. It has already been shown that the map **Q** can capture two conjugate attractors of the Poincaré map **P** (i.e., two conjugate motions in the phase space).[19] Therefore, in this paper, the map **Q** is used to investigate the dynamics of the vibro-impact system, and is called *the virtual Poincaré map*.

Let $\mathbf{T}_\mathbf{Q}(\mathbf{X}) = \mathbf{D}_\mathbf{X}\mathbf{Q}$ denotes the Jacobi matrix of the Poincaré map **Q** at the initial map point **X**, then

$$\mathbf{T}_\mathbf{Q}^N(\mathbf{X}) = \mathbf{T}_\mathbf{Q}(\mathbf{Q}^{N-1}\mathbf{X}) \cdots \mathbf{T}_\mathbf{Q}(\mathbf{Q}\mathbf{X})\mathbf{T}_\mathbf{Q}(\mathbf{X}), \tag{11}$$

where $\mathbf{Q}^k\mathbf{X}$ represents the k th iteration of **Q** at the point **X**. Let Λ_j^N be eigenvalues of the matrix $\mathbf{T}_\mathbf{Q}^N(\mathbf{X})$, the Lyapunov exponents can be computed as[23,24]

$$\lambda_j = \lim_{N\to\infty} \frac{1}{N} \ln|\Lambda_j^N|, \quad j = 1, 2, 3, 4, 5, 6, \tag{12}$$

where the Lyapunov exponents are ranked from large to small as $\lambda_1 \geq \lambda_2 \geq \cdots \geq \lambda_6$.

However, Eq. (11) cannot be used to calculate the Lyapunov exponents directly. The reason for this is that, when the number of iteration of the map **Q** increases, the components of the matrix $\mathbf{T}_\mathbf{Q}^N(\mathbf{x}^*)$ may become infinite for chaotic attractors and null for periodic attractors. To avoid the overflow issue, the **QR** method, as a tool of continuous orthogonalization, is applied repeatedly to the computation.[20,23,24] It is known that[20,24] the largest Lyapunov exponent for a quasi-periodic attractor is zero, and that for a chaotic attractor is positive. However, in this paper we show that for QCs, the largest finite-time Lyapunov exponent[25] does not converge to a constant, but fluctuates in the positive region, which is the result of the fact that the map point enters in turn into quasiperiodic attractors and a chaotic component as the iteration number is increased.

III. SYMMETRIC LIMIT SET AND SYMMETRY RESTORING BIFURCATION

In this paper, it is assumed that $\mathbf{Q}_1$, **Q**, and **P** are all continuous and invertible. The ω-limit sets of **X** generated by the iterations of the **P** map and the **Q** map are denoted by $\omega_\mathbf{P}(\mathbf{X})$ and $\omega_\mathbf{Q}(\mathbf{X})$, respectively. A limit set can be attracting or non-attracting. Here an attractor is defined to be an asymptotically stable ω-limit set.[8] Since **X** and $\mathbf{Q}(\mathbf{X})$ are a pair of conjugate map points, two ω-limits set generated by **X** and $\mathbf{Q}(\mathbf{X})$ (i.e., $\omega_\mathbf{P}(\mathbf{X})$ and $\omega_\mathbf{P}(\mathbf{Q}(\mathbf{X}))$) are called a pair of conjugate ω-limit sets.[8,19]

The positive orbit of the map point **X** under the **Q** map is **X**, $\mathbf{Q}(\mathbf{X})$, $\mathbf{Q}^2(\mathbf{X})$, $\mathbf{Q}^3(\mathbf{X})$,..., $\mathbf{Q}^{2k}(\mathbf{X})$, $\mathbf{Q}^{2k+1}(\mathbf{X})$,.... Since the **P** map is the second iteration of the **Q** map, then we have

$$\mathbf{Q}^{2k}(\mathbf{X}) = \mathbf{P}^k(\mathbf{X}), \tag{13}$$

and

$$\mathbf{Q}^{2k+1}(\mathbf{X}) = \mathbf{P}^k(\mathbf{Q}(\mathbf{X})). \tag{14}$$

That is, the orbit of the map point **X** under the map **P** comes from the even iteration number of the map **Q**, and the orbit of the map point $\mathbf{Q}(\mathbf{X})$ under the map **P** comes from the odd iteration number of the map **Q**. Therefore, Eqs. (13) and (14) imply

$$\omega_{\mathbf{Q}^{2k}}(\mathbf{X}) = \omega_\mathbf{P}(\mathbf{X}), \tag{15}$$

and

$$\omega_{\mathbf{Q}^{2k+1}}(\mathbf{X}) = \omega_\mathbf{P}(\mathbf{Q}(\mathbf{X})), \tag{16}$$

respectively. That is, $\omega_{\mathbf{Q}^{2k}}(\mathbf{X})$ and $\omega_{\mathbf{Q}^{2k+1}}(\mathbf{X})$ represent two conjugate ω-limit sets $\omega_\mathbf{P}(\mathbf{X})$ and $\omega_\mathbf{P}(\mathbf{Q}(\mathbf{X}))$, respectively. Then we have

$$\omega_\mathbf{Q}(\mathbf{X}) = \omega_\mathbf{P}(\mathbf{X}) \cup \omega_\mathbf{P}(\mathbf{Q}(\mathbf{X})). \tag{17}$$

In addition, since

$$\mathbf{Q}(\mathbf{P}^k(\mathbf{X})) = \mathbf{Q}^{2k+1}(\mathbf{X}) = \mathbf{P}^k(\mathbf{Q}(\mathbf{X})), \tag{18}$$

then

$$\lim_{k\to\infty} \mathbf{Q}(\mathbf{P}^k(\mathbf{X})) = \lim_{k\to\infty} \mathbf{P}^k(\mathbf{Q}(\mathbf{X})), \tag{19}$$

that is

$$\mathbf{Q}(\omega_\mathbf{P}(\mathbf{X})) = \omega_\mathbf{P}(\mathbf{Q}(\mathbf{X})). \tag{20}$$

If the ω-limit sets of $\mathbf{Q}^{2k}$ and that of $\mathbf{Q}^{2k+1}$ satisfy[8,19]

$$\omega_{\mathbf{Q}^{2k}}(\mathbf{X}) = \omega_{\mathbf{Q}^{2k+1}}(\mathbf{X}), \tag{21}$$

$\omega_{\mathbf{P}}(\mathbf{X})$, $\omega_{\mathbf{Q}^{2k}}(\mathbf{X})$, $\omega_{\mathbf{Q}^{2k+1}}(\mathbf{X})$, and $\omega_{\mathbf{Q}}(\mathbf{X})$ are all *symmetric limit sets*.

Equation (21) means that, if the ω-limit sets of $\mathbf{X}$ equals to its conjugate limit set, $\omega_{\mathbf{P}}(\mathbf{X})$ is a symmetric limit set. Moreover, an ω-limit set is symmetric if $\mathbf{P}$ and $\mathbf{Q}$ have the same limit set (i.e., $\omega_{\mathbf{P}}(\mathbf{X}) = \omega_{\mathbf{Q}}(\mathbf{X})$). Besides, $\omega_{\mathbf{P}}(\mathbf{X})$ is symmetric if it is mapped onto itself under the $\mathbf{Q}$ map (i.e., $\mathbf{Q}(\omega_{\mathbf{P}}(\mathbf{X})) = \omega_{\mathbf{P}}(\mathbf{X})$).

Here the Poincaré map $\mathbf{P}$ itself does not reflect the symmetry. However, Eqs. (15)–(17) suggest that the non-symmetric implicit map $\mathbf{Q}$ can capture two coexistent conjugate ω-limit sets, which reflect the symmetry of the vibro-impact system.

Proposition 1.[8] if $\omega_{\mathbf{P}}(\mathbf{X})$ is an attractor, and $\omega_{\mathbf{Q}^{2k}}(\mathbf{X}) \cap \omega_{\mathbf{Q}^{2k+1}}(\mathbf{X}) \neq \varnothing$ (i.e., $\omega_{\mathbf{P}}(\mathbf{X}) \cap \mathbf{Q}(\omega_{\mathbf{P}}(\mathbf{X})) \neq \varnothing$), then $\omega_{\mathbf{Q}^{2k}}(\mathbf{X}) = \omega_{\mathbf{Q}^{2k+1}}(\mathbf{X})$ (i.e., $\omega_{\mathbf{P}}(\mathbf{X}) = \mathbf{Q}(\omega_{\mathbf{P}}(\mathbf{X})) = \omega_{\mathbf{Q}}(\mathbf{X})$). That is, $\omega_{\mathbf{P}}(\mathbf{X})$, $\omega_{\mathbf{Q}^{2k}}(\mathbf{X})$, $\omega_{\mathbf{Q}^{2k+1}}(\mathbf{X})$, and $\omega_{\mathbf{Q}}(\mathbf{X})$ are all *symmetric limit sets*.

That is, as a parameter changes, once two conjugate limit sets intersect each other, symmetry restoring bifurcation takes place. It was proved first in Ref. 6 that if $\hbar : \mathbf{R}^n \to \mathbf{R}^n$ is continuous and commutes with a matrix ρ, and $A \in \mathbf{R}^n$ is an attractor and if $A \cap \rho(A) \neq \varnothing$, then $A = \rho(A)$. However, in our case, $\omega_{\mathbf{Q}^{2k}}$ (i.e., $\omega_{\mathbf{P}}(\mathbf{X})$) is dependent on time. Since there is not a single ρ which can take elements in $\omega_{\mathbf{P}}(\mathbf{X})$ to its conjugate, the matrix ρ is replaced by the map $\mathbf{Q}$, and the condition $A \cap \rho(A) \neq \varnothing$ is replaced by $\omega_{\mathbf{P}}(\mathbf{X}) \cap \mathbf{Q}(\omega_{\mathbf{P}}(\mathbf{X})) \neq \varnothing$, equivalently.

In Ref. 8, a general mechanism for symmetry restoring bifurcation has been proposed. That is, when the solutions before and after the bifurcation are attracting, then symmetry restoring bifurcation is the result of a collision (i.e., intersection) between conjugate limit set and a symmetric limit set. In this paper, as shown in the following section, for the six dimensional map $\mathbf{Q}$ shown as Eq. (8), which describes the dynamics of the three degree of freedom vibro-impact system, we discuss three types of symmetry restoring bifurcations according to the way the two conjugate limit sets intersect with each other:

(I) Two conjugate *chaotic* attractors connect with each other directly. In this case chaos-chaos intermittency is induced by the chaotic attractor-merging crisis.

It is known that the collisions of two conjugate chaotic attractors also means that they collide with a saddle unstable orbit (i.e., the unstable symmetric fixed point) on the basin boundary.[4] To detect the critical point of symmetry restoring bifurcation (i.e., attractor-merging crisis in this case), we define a distance sequence between the two conjugate chaotic attractors and the unstable symmetric fixed point $\mathbf{X}^*$,

$$d(N) = \sqrt{(x_1^* - x_{1N})^2 + (y_1^* - y_{1N})^2 + (x_2^* - x_{2N})^2 + (y_2^* - y_{2N})^2 + (x_3^* - x_{3N})^2 + (y_3^* - y_{3N})^2}, \tag{22}$$

where $(x_1^*, y_1^*, x_2^*, y_2^*, x_3^*, y_3^*)$ are the coordinates of $\mathbf{X}^*$, and $(x_{1N}, y_{1N}, x_{2N}, y_{2N}, x_{3N}, y_{3N})$ are the coordinates of map point $\mathbf{X}$ at the Nth iteration. As the iteration number N is increased, there is a distance sequence $\{d(N)\}$. Since $\min\{d(N)\} = 0$ indicates the direct collision between $\omega_{\mathbf{Q}^{2k}}(\mathbf{X})$ and $\omega_{\mathbf{Q}^{2k+1}}(\mathbf{X})$, it can be used to detect the critical point of the attractor-merging crisis.

(II) Two conjugate *quasiperiodic* sets are suddenly embedded in a chaotic set. In this case, QCs are induced by a new intermittency.

For the discrete dynamical systems, four types of attractors are defined in the existing references. They are periodic attractor, quasiperiodic attractor, chaotic attractor, and strange non-chaotic attractor. However, in this paper, we discover a new mixed attractor which is the combination of two conjugate quasiperiodic sets and a chaotic set (see Section IV in detail). Because the size of the quasiperiodic component is always smaller than the chaotic component, we say, that the two quasiperiodic sets are embedded in a chaotic set. Now quasiperiodic chaos (i.e., quasiperiodic chaotic attractor) is defined as follows:

Definition 2. Quasiperiodic chaos (QC) is an attractor which is the combination of quasiperiodic limit sets and a chaotic limit set.

For the two conjugate quasiperiodic sets, a map iteration cannot visit directly from one to another because they have no intersection. However, the appearance of the chaotic set makes the transition possible. Therefore, the iteration interval of the chaotic set is always between the two conjugate quasiperiodic sets. Now for map $\mathbf{Q}^{2k}$, pick three iteration intervals $I_1 = (s_1, s + s_1]$, $I_2 = (s + s_1, s + s_1 + s_2]$, and $I_3 = (s + s_1 + s_2, s + s_1 + s_2 + s_3]$, where s, s_1, s_2, and s_3 are positive integers, and $s_1 = s_3$. As $s \to +\infty$, let $\omega_{\mathbf{Q}^{2k}}^{I_1}(\mathbf{X})$, $\omega_{\mathbf{Q}^{2k}}^{I_2}(\mathbf{X})$, and $\omega_{\mathbf{Q}^{2k}}^{I_3}(\mathbf{X})$ be three components of the ω-limit sets of the map $\mathbf{Q}^{2k}$ corresponding to the iteration interval I_1, I_2, and I_3, respectively. That is, $\omega_{\mathbf{Q}^{2k}}^{I_1}(\mathbf{X})$ and $\omega_{\mathbf{Q}^{2k}}^{I_3}(\mathbf{X})$ are two conjugate sets, and $\omega_{\mathbf{Q}^{2k}}^{I_2}(\mathbf{X})$ is the chaotic set. The following proposition strictly proves that the appearance of a mixed limit set means that symmetry restoring bifurcation takes place at the same time.

Proposition 3. If $\omega_{\mathbf{Q}^{2k}}(\mathbf{X})$ (or $\omega_{\mathbf{Q}^{2k+1}}(\mathbf{X})$) contains two conjugate sets $\omega_{\mathbf{Q}^{2k}}^{I_1}(\mathbf{X})$ and $\omega_{\mathbf{Q}^{2k}}^{I_3}(\mathbf{X})$, which do not necessarily intersect, and a chaotic set $\omega_{\mathbf{Q}^{2k}}^{I_2}(\mathbf{X})$, then $\omega_{\mathbf{Q}}(\mathbf{X})$, $\omega_{\mathbf{Q}^{2k}}(\mathbf{X})$, and $\omega_{\mathbf{Q}^{2k+1}}(\mathbf{X})$ are all symmetric, and

$$\omega_{\mathbf{Q}^{2k}}(\mathbf{X}) \cap \omega_{\mathbf{Q}^{2k+1}}(\mathbf{X}) \supset \omega_{\mathbf{Q}^{2k}}^{I_1}(\mathbf{X}) \cup \omega_{\mathbf{Q}^{2k}}^{I_3}(\mathbf{X}) \neq \varnothing. \tag{23}$$

Proof. Since $\omega_{\mathbf{Q}^{2k}}(\mathbf{X})$ is a mixed set containing three components, then

$$\omega_{\mathbf{Q}^{2k}}(\mathbf{X}) = \omega^{I_1}_{\mathbf{Q}^{2k}}(\mathbf{X}) \cup \omega^{I_2}_{\mathbf{Q}^{2k}}(\mathbf{X}) \cup \omega^{I_3}_{\mathbf{Q}^{2k}}(\mathbf{X}). \quad (24)$$

Because $\omega^{I_1}_{\mathbf{Q}^{2k}}(\mathbf{X})$ and $\omega^{I_3}_{\mathbf{Q}^{2k}}(\mathbf{X})$ are two conjugate sets, then

$$\mathbf{Q}(\omega^{I_1}_{\mathbf{Q}^{2k}}(\mathbf{X})) = \omega^{I_3}_{\mathbf{Q}^{2k}}(\mathbf{X}). \quad (25)$$

Equation (24) implies

$$\omega_{\mathbf{Q}^{2k}}(\mathbf{X}) \supset \omega^{I_1}_{\mathbf{Q}^{2k}}(\mathbf{X}), \quad (26)$$

hence

$$\mathbf{Q}(\omega_{\mathbf{Q}^{2k}}(\mathbf{X})) \supset \mathbf{Q}(\omega^{I_1}_{\mathbf{Q}^{2k}}(\mathbf{X})). \quad (27)$$

According to Eq. (25), Eq. (27) can be rewritten as

$$\omega_{\mathbf{Q}^{2k+1}}(\mathbf{X}) \supset \omega^{I_3}_{\mathbf{Q}^{2k}}(\mathbf{X}). \quad (28)$$

Similarly, because

$$\omega_{\mathbf{Q}^{2k}}(\mathbf{X}) \supset \omega^{I_3}_{\mathbf{Q}^{2k}}(\mathbf{X}), \quad (29)$$

and

$$\omega^{I_1}_{\mathbf{Q}^{2k}}(\mathbf{X}) = \mathbf{Q}(\omega^{I_3}_{\mathbf{Q}^{2k}}(\mathbf{X})), \quad (30)$$

we obtain

$$\omega_{\mathbf{Q}^{2k+1}}(\mathbf{X}) \supset \omega^{I_1}_{\mathbf{Q}^{2k}}(\mathbf{X}). \quad (31)$$

According to Eqs. (26), (28), (29), and (31), we prove Eq. (23). Then, based on Proposition 1, $\omega_{\mathbf{Q}}(\mathbf{X})$, $\omega_{\mathbf{Q}^{2k}}(\mathbf{X})$, $\omega_{\mathbf{Q}^{2k+1}}(\mathbf{X})$ are all symmetric limit sets since $\omega_{\mathbf{Q}^{2k}}(\mathbf{X}) \cap \omega_{\mathbf{Q}^{2k+1}}(\mathbf{X}) \neq \varnothing$. If $\omega_{\mathbf{Q}^{2k+1}}(\mathbf{X})$ is a mixed set containing two conjugate sets and a chaotic set, the proof is similar to the above. ■

Remark: A variant version of Proposition 3 was proved first in Ref. 8. Proposition 9 in Ref. 8 shows that if an ω- limit set contains two (or more) conjugate sets it also intersects with its own conjugate set.

1. For Proposition 9 in Ref. 8, the initial conditions of the two conjugate sets $\omega_{\mathbf{P}}(\mathbf{y})$, $\omega_{\mathbf{P}}(\mathbf{Q}(\mathbf{y}))$ are different from that of $\omega_{\mathbf{P}}(\mathbf{x})$, which are represented by $\mathbf{y}$ and $\mathbf{x}$, respectively. However, here the initial conditions of two conjugate sets $\omega^{I_1}_{\mathbf{Q}^{2k}}(\mathbf{X})$ and $\omega^{I_3}_{\mathbf{Q}^{2k}}(\mathbf{X})$ are the same as that of $\omega^{I_2}_{\mathbf{Q}^{2k}}(\mathbf{X})$, which are all represented by $\mathbf{X}$. This implies that, $\omega^{I_1}_{\mathbf{Q}^{2k}}(\mathbf{X})$, $\omega^{I_2}_{\mathbf{Q}^{2k}}(\mathbf{X})$, and $\omega^{I_3}_{\mathbf{Q}^{2k}}(\mathbf{X})$ are all the parts of a single limit set, but not three independently limit sets. Then, as the iteration number tends to be infinite, the iteration interval is divided into three infinitely repeated sections I_1, I_2, and I_3, and the map point must alternate among $\omega^{I_1}_{\mathbf{Q}^{2k}}(\mathbf{X})$, $\omega^{I_2}_{\mathbf{Q}^{2k}}(\mathbf{X})$, and $\omega^{I_3}_{\mathbf{Q}^{2k}}(\mathbf{X})$ correspondingly, indicating a new intermittency.
2. Based on the numerical results shown in Section IV, here $\omega^{I_1}_{\mathbf{Q}^{2k}}(\mathbf{X})$ and $\omega^{I_3}_{\mathbf{Q}^{2k}}(\mathbf{X})$ are defined clearly as two conjugate quasiperiodic sets and $\omega^{I_2}_{\mathbf{Q}^{2k}}(\mathbf{X})$ is defined as the chaotic set. However, the whole contents in Ref. 8 have discussed only periodic sets and chaotic sets, but not quasiperiodic sets.
3. $\omega^{I_1}_{\mathbf{Q}^{2k}}(\mathbf{X})$ and $\omega^{I_3}_{\mathbf{Q}^{2k}}(\mathbf{X})$ have no intersection. Transition between the two conjugate quasiperiodic sets depends always on the chaotic set $\omega^{I_2}_{\mathbf{Q}^{2k}}(\mathbf{X})$. Therefore, the iteration interval of the chaotic set I_2 is always between the two conjugate quasiperiodic sets. And the chaotic set $\omega^{I_2}_{\mathbf{Q}^{2k}}(\mathbf{X})$ must be between two conjugate quasiperiodic sets. Because the two quasiperiodic sets are conjugate (i.e., Eq. (25) stands), I_1 must be equal to I_3, which means $s_1 = s_3$.

In this case, two conjugate limit sets do not connect with each other directly (i.e., $\min\{d(N)\} \neq 0$), but the condition $\omega_{\mathbf{Q}^{2k}}(\mathbf{X}) \cap \omega_{\mathbf{Q}^{2k+1}}(\mathbf{X}) \neq \varnothing$ is also satisfied. Here the intersection of $\omega_{\mathbf{Q}^{2k}}(\mathbf{X})$ and $\omega_{\mathbf{Q}^{2k+1}}(\mathbf{X})$ is exactly the two conjugate quasiperiodic attractors. Therefore, symmetry restoring bifurcation takes place at this critical point. As suggested in Ref. 8, this symmetry restoring bifurcation is still the result of the collision between conjugate limit sets and a symmetric limit set. However, here the symmetric limit set is not the unstable symmetric fixed point $\mathbf{X}^*$, but may be an unstable symmetric multi-periodic points, an unstable quasiperiodic limit set, or an unstable chaotic limit set.

(III) Two conjugate *quasiperiodic* attractors contact with each other directly. In this case, two conjugate quasiperiodic attractors merge to form a single symmetric quasiperiodic attractor (SQA). Contrasted with the above two cases, there is no intermittency after symmetry restoring bifurcation.

It has been shown in Refs. 2–5, 7, and 8 that two conjugate attractors that undergo symmetry restoring bifurcation may be periodic or chaotic. However, in this paper, we show that two conjugate *quasiperiodic* attractors can also undergo symmetry restoring bifurcation, which leads to a QC (the second case) or a single symmetric quasiperiodic attractor (the third case).

IV. SYMMETRY RESTORING BIFURCATIONS AND QCS CAUSED BY A NEW INTERMITTENCY

In this section, we consider the six dimensional virtual implicit Poincaré map $\mathbf{Q}$ shown as Eq. (8). We use Matlab to write programmes to generate all the figures, but do not use the existing solver packages such us Runge-Kuta package. First of all, we use a programme to numerically approach the time between the two consecutive impacts. This time is also the solution of Eq. (10). Then we substitute this time into Eq. (8), and can simulate the process of vibro-impact subsequently. Three types of symmetry restoring bifurcations are analyzed. First, two conjugate chaotic attractors connect with each other directly, which leads to the chaos-chaos intermittency. Second, two conjugate quasiperiodic sets are suddenly embedded in a chaotic set, which leads to a new intermittency between two conjugate quasiperiodic sets and a chaotic set. Third, two conjugate quasiperiodic attractors connect with each other directly and merge to form a single symmetric quasiperiodic attractor.

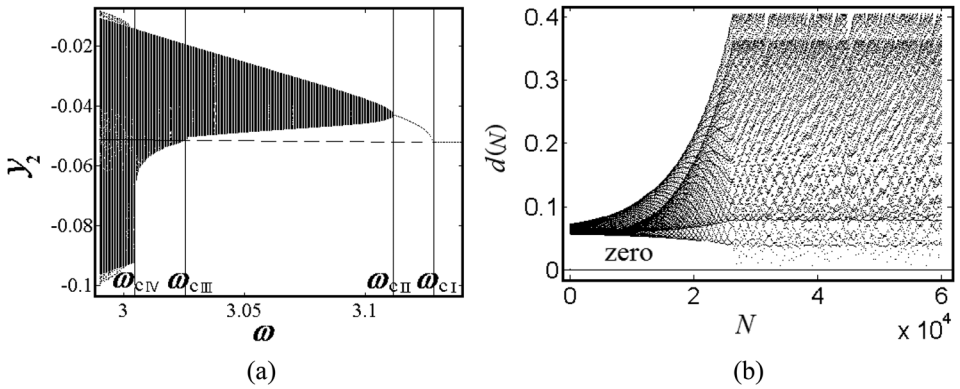

FIG. 2. Detecting attractor merging crisis: (a) bifurcation diagram with the changing parameter ω ($\mathbf{Q}^{2k}$) and (b) the distance d versus iteration number N.

A. Two conjugate chaotic attractors connect with each other directly

Consider the vibro-impact system with system parameters (1): $n = 1$, $\zeta = 0.0086$, $r = 0.85$, $h = 0.06$, $u_{m3} = 0.6$, $u_{m2} = 2.8$, $u_{m1} = 1$, $u_{k3} = 0.8$, $u_{k2} = 0.2$, $u_{k1} = 1$, $u_{f3} = 0.4$, $u_{f2} = 0.5$, $u_{f1} = 1$, and the exciting frequency ω is chosen as the control parameter. Figure 2 represents bifurcation diagram of $\mathbf{Q}^{2k}$ and the distance sequence $\{d(N)\}$. As ω is decreased continuously, the system first undergoes symmetry breaking of symmetric periodic orbit at $\omega_{CI} = 3.127622$. Then a conjugate periodic orbit bifurcates into conjugate quasiperiodic orbit at ω_{CII}, and it evolves into conjugate chaotic attractor via torus doubling subsequently, see Fig. 2(a). After symmetry breaking, the symmetric periodic orbit becomes unstable, and is represented by a dash line. At $\omega_{CIV} = 3.0041$, the attractor exhibits discontinuity abruptly, indicating the attractor-merging crisis. The $\min\{d(N)\}$ is very close to zero at $\omega = 3.0042$, indicating that ω_{CIV} is indeed the attractor merging crisis, see Fig. 2(b). It should be noted that in Fig. 2(a), the attractor-merging crisis occurs at ω_{CIV}, but not at ω_{CIII}. It seems that conjugate attractor connect with the unstable symmetric periodic orbit at ω_{CIII}. However, computation shows that $\min\{d(N)\}$ at ω_{CIII} is far away from zero, indicating that ω_{CIII} is not the attractor-merging crisis. The phase space of the map $\mathbf{Q}$ or $\mathbf{P}$ has six dimensions, but Fig. 2(a) only gives one coordinate y_2. Therefore, generally, $\min\{d(N)\}$ is not zero at ω_{CIII}.

Figure 3 shows the birth of intermittency-induced by attractor-merging crisis. To obtain the phase portrait of the map $\mathbf{Q}$, we need to add a perturbation $\Delta\mathbf{X}$ to the unstable symmetric fixed point $\mathbf{X}^*$ computed in Section III, and iterate map $\mathbf{Q}$ at the initial point $\mathbf{X} = \mathbf{X}^* + \Delta\mathbf{X}$. Attractor of the odd number of iterations (i.e., $\omega_{\mathbf{Q}^{2k+1}}(\mathbf{X})$) is denoted by red points, and that of the even number of iteration (i.e., $\omega_{\mathbf{Q}^{2k}}(\mathbf{X})$) is denoted by blue points. At $\omega = 3.0042$, there are two conjugate chaotic attractors (Fig. 3(a)), and the intermittency does not occur (Fig. 3(b)). At $\omega = 3.0041$, there is only one symmetric chaotic attractor (Fig. 3(c)), and the chaos-chaos intermittency is induced by attractor-merging

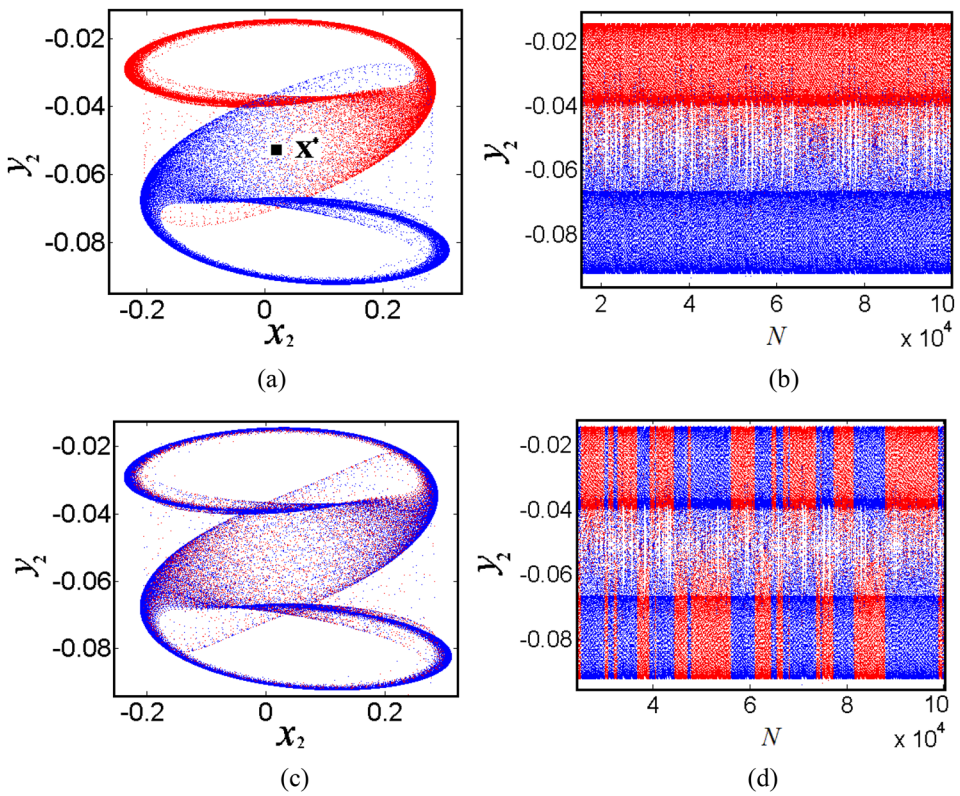

FIG. 3. Birth of intermittency induced by attractor-merging crisis: (a) $\omega = 3.0042$: phase portrait in (x_2, y_2) plane: map $\mathbf{Q}$, (b) $\omega = 3.0042$: y_2 versus iteration number N, (c) $\omega = 3.0041$: phase portrait in (x_2, y_2) plane: map $\mathbf{Q}$, and (d) $\omega = 3.0041$: y_2 versus iteration number N.

crisis (Fig. 3(d)). It should be mentioned that in Fig. 3(a), it seems that two conjugate chaotic attractors have already collided with the unstable symmetric fixed point $\mathbf{X}^*$. However, the overlapping of the two conjugate attractors in the (x_2, y_2) plane cannot determine whether the collision has already taken place or not, because the two dimensional phase portrait is only the projection of the six dimensional phase space.

B. Two conjugate quasiperiodic sets are suddenly embedded in a chaotic set

Consider the vibro-impact system with system parameters (2): $n = 1$, $\zeta = 0.008$, $r = 0.8$, $h = 0.04$, $u_{m3} = 0.45$, $u_{m2} = 2.5$, $u_{m1} = 1$, $u_{k3} = 0.8$, $u_{k2} = 0.5$, $u_{k1} = 1$, $u_{f3} = 0.5$, $u_{f2} = 1$, $u_{f1} = 1$, and the exciting frequency ω chosen as the control parameter. Figure 4 represents the discontinuity of attractor as ω is varied. Bifurcation diagram in the interval $[2.785, 2.995]$ is shown in Fig. 4(a). In the first case shown in Fig. 2(a), there is only one discontinuous point at ω_{CIV}. In contrast, in this case, there are two discontinuous points $\omega_{CA} = 2.799111659$ and $\omega_{CB} = 2.79379$, see Fig. 4(a). The largest Lyapunov exponent changes abruptly at two critical points ω_{CA} and ω_{CB}, implying the singularity of the dynamical behavior, see Fig. 4(b). While $\omega < \omega_{CB}$ and $\omega > \omega_{CA}$, the largest Lyapunov exponent is $\lambda_1 = 0$, indicating that the attractor is quasiperiodic. As $\omega \in [\omega_{CB}, \omega_{CA}]$, the largest Lyapunov exponent is positive, and the second largest Lyapunov exponent is still zero. However, by the following analysis, we show that the attractor in this small parameter interval $[\omega_{CB}, \omega_{CA}]$ is not a pure chaotic attractor, but a new mixed attractor, which is the combination of quasiperiodic set and chaotic set. We name this type of attractor *quasiperiodic chaos attractor* (QC).

For $\omega = \omega_{CA} + 10^{-9}$ and $\omega = \omega_{CA}$, Fig. 5 represents the projected phase portraits in the Poincaré section ($x_2 - y_2$ plane). At $\omega = \omega_{CA} + 10^{-9}$, for the map $\mathbf{Q}^{2k}$ or $\mathbf{Q}^{2k+1}$, there is only one of two conjugate quasiperiodic sets, respectively, see Figs. 5(a) and 5(c). However, for map $\mathbf{Q}$, two conjugate quasiperiodic sets are captured simultaneously, see Fig. 5(e). As ω is decreased to $\omega = \omega_{CA}$, the phase portraits of $\mathbf{Q}$, $\mathbf{Q}^{2k}$ and $\mathbf{Q}^{2k+1}$ are shown in Figs. 5(b), 5(d), and 5(f), respectively. For $\mathbf{Q}^{2k}$, two conjugate quasiperiodic sets and another chaotic set appear simultaneously, see Fig. 5(b). The same thing occurs for $\mathbf{Q}^{2k+1}$, see Fig. 5(d). Moreover, as shown in Figs. 5(b) and 5(d), there is $\omega_{\mathbf{Q}^{2k}}(\mathbf{X}) = \omega_{\mathbf{Q}^{2k+1}}(\mathbf{X})$, indicating that the attractor of $\omega = \omega_{CA}$ is symmetric. In addition to two conjugate quasiperiodic sets, another chaotic set appears suddenly. The attractor shown in Figs. 5(b), 5(d), and 5(f) is not a pure quasi-periodic attractor, nor a pure chaotic one, but a combination of two conjugate quasiperiodic sets and a chaotic set, named QC. In other words, two conjugate quasiperiodic sets are suddenly embedded in a chaotic set at ω_{CA}. Since $\omega_{\mathbf{Q}^{2k}}(\mathbf{X}) \cap \omega_{\mathbf{Q}^{2k+1}}(\mathbf{X}) \neq \varnothing$ (i.e., the intersection is the two conjugate quasiperiodic sets), the attractor changes from non-symmetric at $\omega = \omega_{CA} + 10^{-9}$ to symmetric at $\omega = \omega_{CA}$, indicating that the symmetry restoring bifurcation takes place at this point.

In the two cases of $\omega = \omega_{CA}$ and $\omega = \omega_{CA} - 10^{-9}$, the distance sequence $\{d(N)\}$ between the two conjugate quasiperiodic attractors and the symmetric unstable fixed point $\mathbf{X}^*$ is shown in Figs. 6(a) and 6(b), respectively. Since two conjugate quasiperiodic sets are embedded in the chaotic one, one can distinguish the chaotic interval from the quasiperiodic interval of iteration in Fig. 6. It is shown that with the increasing iteration number, the map point alternates between the two conjugate quasiperiodic sets and the chaotic one. Therefore, QC is caused by the intermittency between two conjugate quasiperiodic sets and a chaotic one. As ω decreases to $\omega = \omega_{CA} - 10^{-9}$, the frequency with which the map iteration points enter into the chaotic set increases, see Fig. 6(b).

It is necessary to analyze the intermittency between the quasiperiodic set and the chaotic one in detail. Now pick $\omega = \omega_{CA} - 4 \times 10^{-9}$. Fig. 7 shows y_2 versus iteration number N, according to which one can observe the intermittency. Now the upper conjugate quasiperiodic attractor is denoted by "QA_1," the lower conjugate one is denoted by "QA_2," and the chaotic component is denoted by CA. As shown in Figs. 7(a) and 7(b), for the map $\mathbf{Q}^{2k}$ (or $\mathbf{Q}^{2k+1}$), since the two conjugate quasiperiodic sets do not intersect with each other, the map point on QA_1 (or QA_2) cannot enter into QA_2 (or QA_1) directly. Hence the chaotic set is the necessary transition between the two conjugate quasiperiodic sets, and the intermittency occurs between QA_1, CA, and QA_2. However, for the map $\mathbf{Q}$, the intermittency occurs between two conjugate quasiperiodic sets and the chaotic one, see Fig. 7(c). Fig. 8 shows the projected phase portraits in the Poincaré section ($x_2 - y_2$ plane). As the iteration number N is increased infinitely, for the map $\mathbf{Q}^{2k}$ (or $\mathbf{Q}^{2k+1}$), the sequence of the limit

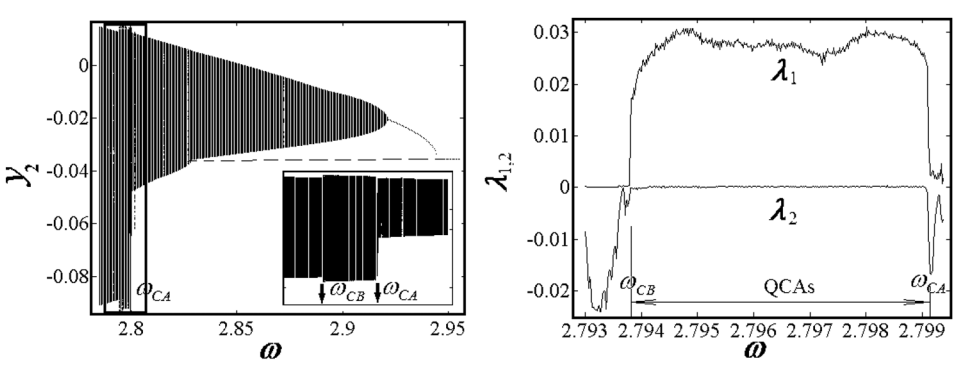

FIG. 4. Discontinuity of attractor. (a) Bifurcation diagram and the enlargement of the red box and (b) Lyapunov exponents $\lambda_{1,2}$ in the interval $[\omega_{CB}, \omega_{CA}]$.

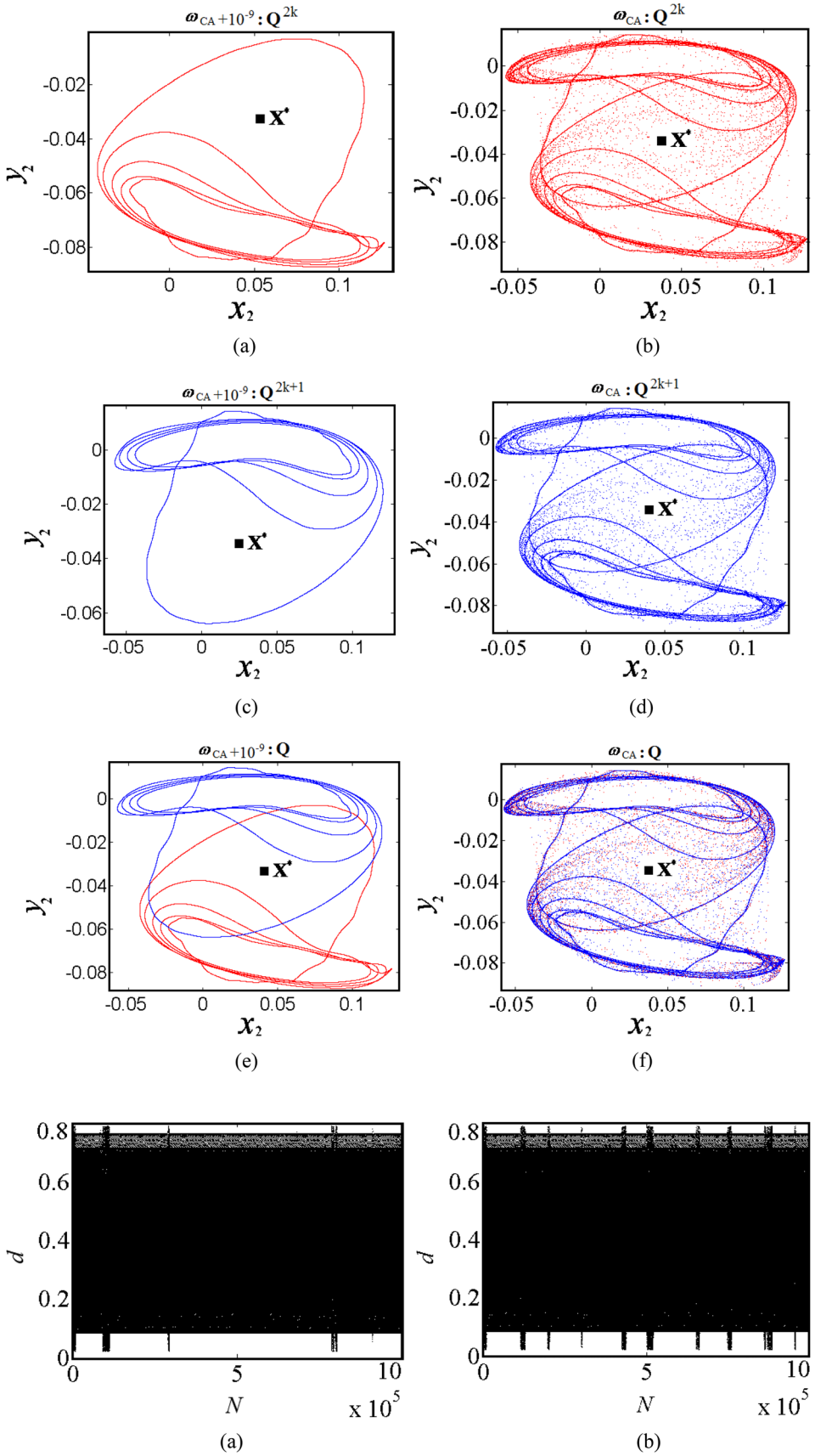

FIG. 5. The projected phase portraits in the Poincaré section ($x_2 - y_2$ plane). (a) $\omega = \omega_{CA} + 10^{-9}$: $\mathbf{Q}^{2k}$, (b) $\omega = \omega_{CA}$: $\mathbf{Q}^{2k}$, (c) $\omega = \omega_{CA} + 10^{-9}$: $\mathbf{Q}^{2k+1}$, (d) $\omega = \omega_{CA}$: $\mathbf{Q}^{2k+1}$, (e) $\omega = \omega_{CA} + 10^{-9}$: $\mathbf{Q}$, and (f) $\omega = \omega_{CA}$: $\mathbf{Q}$.

FIG. 6. The distance d with the changing iteration number N. (a) $\omega = \omega_{CA}$ and (b) $\omega = \omega_{CA} - 10^{-9}$.

set is $QA_1 \rightarrow CA \rightarrow QA_2 \rightarrow CA \rightarrow QA_1 \rightarrow \cdots$, see Fig. 8(a). However, for the map **Q**, if QAs is used to denote two conjugate quasiperiodic sets (i.e., $QA_1 + QA_2$), the sequence of the limit set is QAs → CA → QAs → CA →···, see Fig. 8(b).

It is known that the largest Lyapunov exponent for a quasiperiodic attractor is zero, and that for a chaotic attractor is positive. For the QC, the map point alternates between the two types of sets (chaotic set and quasiperiodic

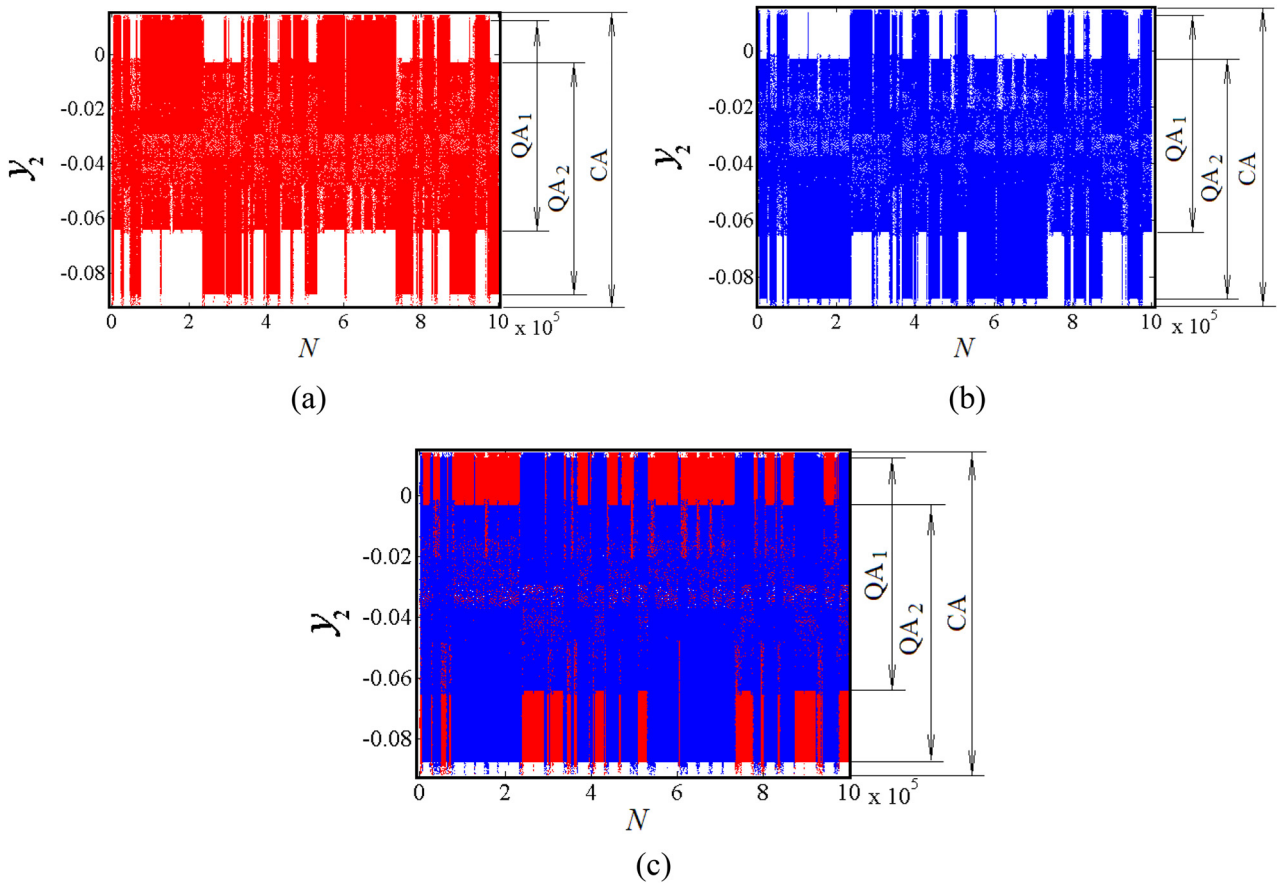

FIG. 7. Intermittency between the quasiperiodic sets and the chaotic one ($\omega = \omega_{CA} - 4 \times 10^{-9}$): y_2 versus iteration number N. (a) $\mathbf{Q}^{2k}$, (b) $\mathbf{Q}^{2k+1}$, and (c) $\mathbf{Q}$.

set), hence the largest finite-time Lyapunov exponent fluctuates in the positive region at $\omega = \omega_{CA} - 4 \times 10^{-9}$, see Fig. 9(a). Fig. 9(b) is the enlargement of the box in Fig. 9(a), and shows the fluctuations of the largest finite-time Lyapunov exponent. That is, the property of QC determines that there is not a convergent largest Lyapunov exponent.

C. Two conjugate quasiperiodic attractors connect with each other directly

Consider still the parameter combination (2). As ω is decreased to some value, the two conjugate quasiperiodic attractors in the QC bifurcate into two larger ones which are very close to each other, and it is still embedded into a chaotic attractor. For example, at $\omega = \omega_{CB} = 2.79379$, the new

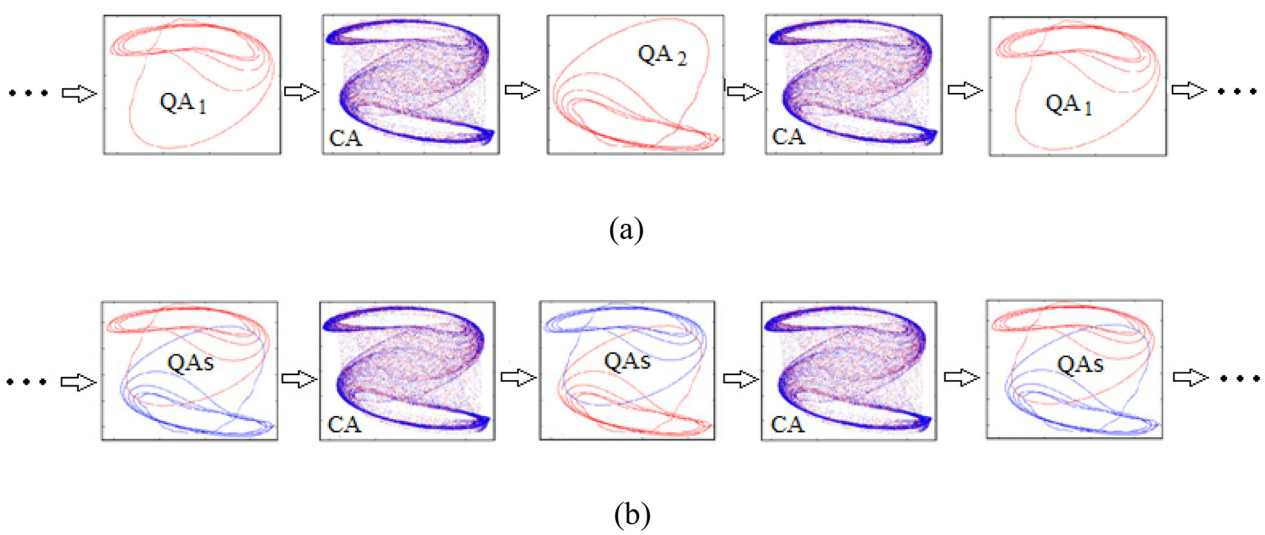

FIG. 8. Projected phase portraits in the Poincaré section ($x_2 - y_2$ plane) as the iteration number N is increased infinitely: $\omega = \omega_{CA} - 4 \times 10^{-9}$. (a) $\mathbf{Q}^{2k}$: the map point alternates QA_1, CA, and QA_2 and (b) $\mathbf{Q}$: the map point alternates between QAs and CA.

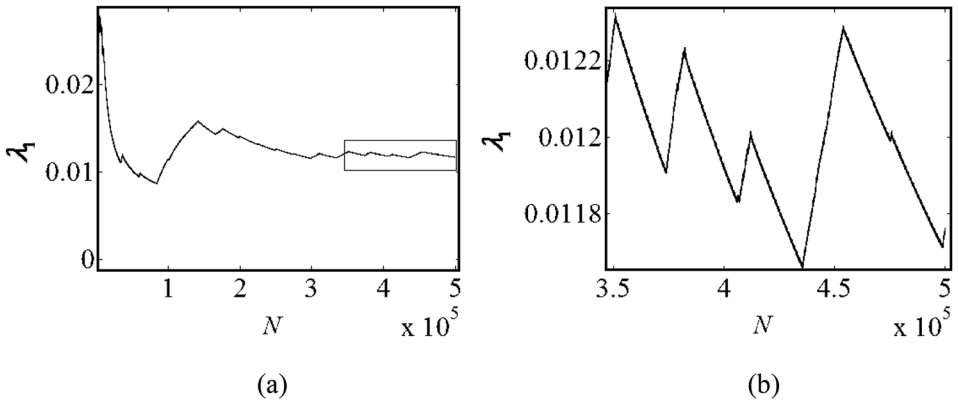

FIG. 9. The largest Lyapunov exponent with the changing iteration number: $\omega = \omega_{CA} - 4 \times 10^{-9}$. (a) 50 0000 iterations, (b) iteration interval: 35 0000–50 0000, which is the enlargement of the box in (a).

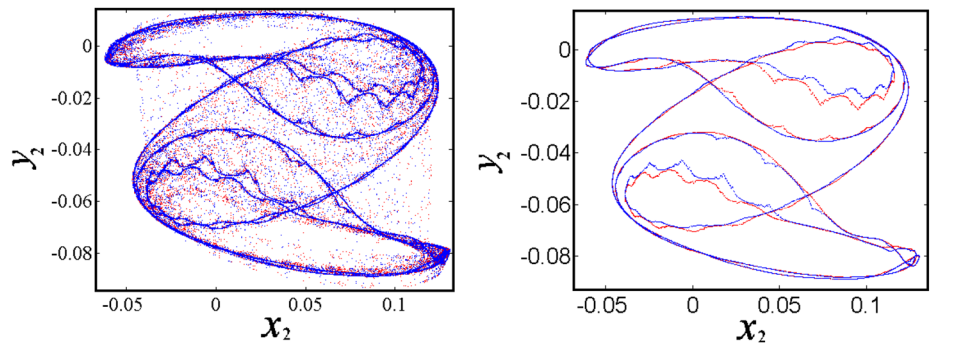

FIG. 10. $\omega = \omega_{CB}$: (a)–(c) Phase portraits in the (x_2, y_2) plane: map **Q** and (d) intermittency: d versus iteration number N.

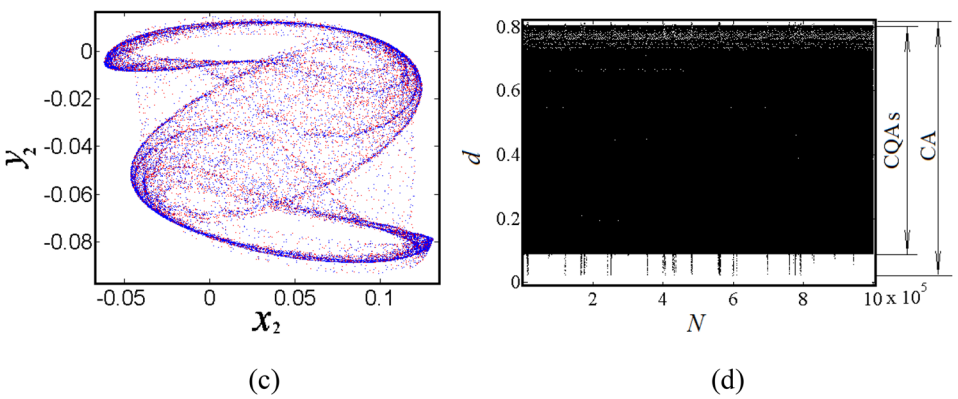

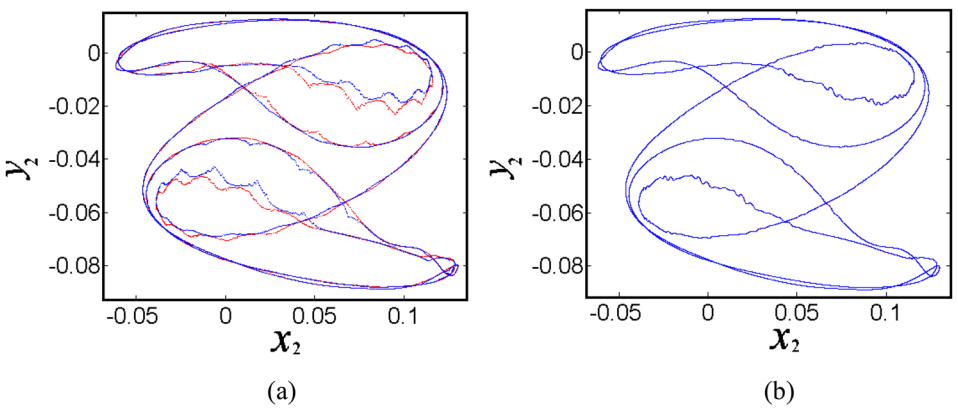

FIG. 11. Phase portraits in the (x_2, y_2) plane: map **Q**. (a) $\omega = \omega_{CB} - 10^{-5}$: two conjugate quasiperiodic attractors and (b) $\omega = \omega_{CB} - 10^{-4}$: symmetric quasiperiodic attractor.

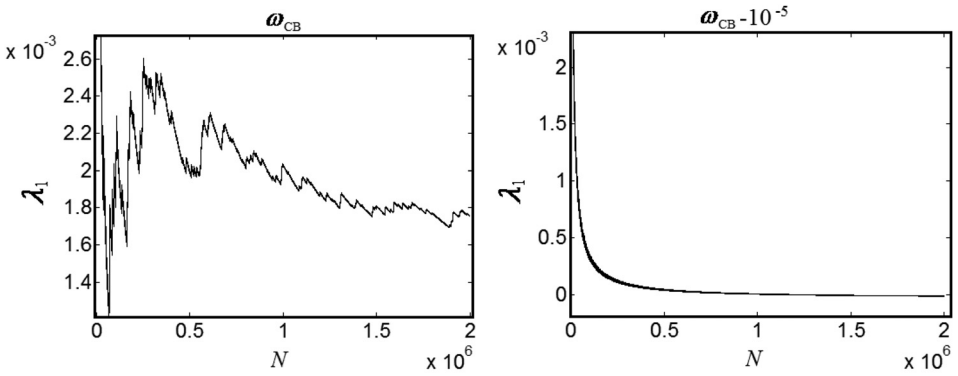

(a) (b)

FIG. 12. The largest Lyapunov exponent with the changing iteration number. (a) $\omega = \omega_{CB}$ and (b) $\omega = \omega_{CB} - 10^{-5}$.

QC is shown in Fig. 10(a). Figs. 10(b) and 10(c) represent the two conjugate quasiperiodic attractors and the chaotic one in the QC, respectively. Fig. 10(d) shows the intermittency between two conjugate quasiperiodic attractors and the chaotic one.

However, as ω is decreased to $\omega = \omega_{CB} - 10^{-5}$, the chaotic component disappears abruptly, and the previous QC bifurcates into two pure conjugate quasiperiodic attractors, indicating that symmetry breaking bifurcation takes place, see Fig. 11(a). Here two conjugate quasiperiodic attractors are close to each other, but do not intersect with each other yet. However, as ω is decreased to $\omega = \omega_{CB} - 10^{-4}$, two conjugate quasiperiodic attractors connect with each other and merge to form a single *symmetric* quasiperiodic attractor (SQA), implying that symmetry restoring bifurcation occurs again, see Fig. 11(b). However, here it should be noted that the SQA shown as Fig. 11(b) has no intermittency.

The largest Lyapunov exponents in the two cases of $\omega = \omega_{CB}$ and $\omega = \omega_{CB} - 10^{-5}$ are shown in Figs. 12(a) and 12(b), respectively. In the case of $\omega = \omega_{CB}$, the system exhibits a quasiperiodic chaos; hence, the curve of the largest Lyapunov exponent fluctuates in the positive region, see Fig. 12(a). By contrast, in the case of $\omega = \omega_{CB} - 10^{-5}$, the system exhibits two pure conjugate quasiperiodic attractors; hence, the curve of the largest Lyapunov exponent converges smoothly to zero, see Fig. 12(b).

V. CONCLUSIONS

The Poincaré map **P** is the 2-fold composition of another virtual implicit map **Q**, governing the symmetry of the three-degree of freedom vibro-impact system. Since map **Q** can exhibit the presence of two conjugate attractors, it is used to investigate the dynamical behaviour of the system. Three types of symmetry restoring bifurcations are identified. First, if two conjugate chaotic attractors contact with each other directly (i.e., $\min\{d(N)\} = 0$), the chaos-chaos intermittency induced by attractor-merging crisis takes place. Second, if two conjugate quasiperiodic sets are suddenly embedded in a chaotic set, QC is induced by a new intermittency. Third, if two conjugate quasiperiodic attractors connect with each other directly, they will merge to form a single symmetric quasiperiodic attractor.

For the second case, since the two conjugate quasiperiodic sets are embedded into the chaotic one, the distance sequence $\{d(N)\}$ between the two conjugate quasiperiodic sets and the unstable symmetric fixed point $\mathbf{X}^*$ can be used to characterize this intermittency. The two conjugate quasiperiodic sets do not intersect with each other, hence the map iteration points cannot jump from one to another directly. However, the appearance of the chaotic set makes it possible. Therefore, the chaotic component of the QC plays a key role in this special intermittency.

The fact that QC contains two conjugate quasiperiodic sets means that $\omega_{\mathbf{Q}^{2k}} \cap \omega_{\mathbf{Q}^{2k+1}} \neq \varnothing$. Hence, the appearance of QC implies that symmetry restoring bifurcation has taken place. Besides, the largest Lyapunov exponent of the QC does not converge to a constant, but fluctuates in the positive region, corresponding to the fact that the map point alternates between the two conjugate quasiperiodic sets and the chaotic one.

As shown in the second and the third cases, the transition to symmetric quasiperiodic attractor is: two conjugate quasiperiodic attractors → QC → two larger conjugate quasiperiodic attractors → one symmetric quasiperiodic attractor. Here, the QC plays the key role in the transition from two conjugate quasiperiodic attractors to symmetric quasiperiodic one. To our knowledge, QC has not been reported in the literature up to now. We believe that the discovery of QC has major significance for both the study of the symmetry restoring bifurcation in high dimensional nonlinear dynamical system and the optimal design of the multi-degree of freedom vibro-impact system.

The appearing (or disappearing) of QC is always accompanied with symmetry restoring (or symmetry breaking). As suggested in Ref. 8, we believe that the birth of QC is related to the collision between two conjugate quasiperiodic attractors and some unstable symmetric limit set. Therefore, the intermittency between two conjugate quasiperiodic sets and the chaotic set does not belong to one of the three classical intermittencies shown in Refs. 1–3. However, here the unstable symmetric limit set cannot be the unstable symmetric fixed point $\mathbf{X}^*$, since $\min\{d_N\} \neq 0$ at the critical point. We conjecture that it may be the unstable symmetric multi-period points, the unstable chaotic limit set, or the unstable quasiperiodic limit set. Unfortunately, because the map **Q** or

P is a six dimensional *implicit* map (i.e., without explicit expression), some analytical methods used in low-order systems, with explicit expressions shown in Refs. 2–4, 6, and 7, cannot be applied to the three-degree of freedom vibro-impact system. Although there are some methods to search for unstable period orbits[9] and chaotic saddles[26] in many low-dimensional dynamical systems, it is not easy to determine the possible unstable symmetric limit set for the same reason. Therefore, the dynamical characterization of this unstable symmetric limit set in multi-degree of freedom vibro-impact systems, remains an open topic for research. Besides, it should be mentioned that the third case shows that not all symmetry restoring bifurcations lead to intermittency.

ACKNOWLEDGMENTS

This work was supported by National Natural Science Foundation of China (11272268, 11572263, and 11672249).

[1]Y. Pomeau and P. Manneville, Commun. Math. Phys. **74**, 189 (1980).
[2]C. Grebogi, E. Ott, and J. A. Yorke, Phys. Rev. Lett. **48**, 1507 (1982).
[3]C. Grebogi, E. Ott, and J. A. Yorke, Physica D **7**, 181 (1983).
[4]C. Grebogi, E. Ott, F. Romeiras, and J. A. Yorke, Phys. Rev. A **11**, 5365 (1987).
[5]V. Tchistiakov, Physical D **91**, 67 (1996).
[6]P. Chossat and M. Golubitsky, Physica D **32**, 423 (1988).
[7]C. Robert, K. T. Alligood, E. Ott, and J. A. York, Physical D **144**, 44 (2000).
[8]A. Ben-Tal, Physica D **171**, 236 (2002).
[9]R. L. Davidchack and Y. C. Lai, Phys. Rev. E **60**(5), 6172 (1999).
[10]C. Grebogi, E. Ott, F. Romeiras, and J. A. Yorke, Phys. Rev. A **37**, 1711 (1988).
[11]P. J. Holmes, J. Sound Vib. **84**, 173 (1982).
[12]A. C. J. Luo, Chaos, Solitons Fractals **19**, 823 (2004).
[13]J. H. Xie and W. C. Ding, Int. J. Nonlinear Mech. **40**, 531 (2005).
[14]W. C. Ding and J. H. Xie, J. Sound Vib. **287**, 101 (2005).
[15]Y. Yue and J. H. Xie, Int. J. Nonlinear Mech. **48**, 51 (2013).
[16]Y. X. Zhang, G. Q. Kong, and J. N. Yin, Acta Phys. Sin. **57**(10), 6182 (2008) (in Chinese).
[17]A. B. Nordmark, J. Sound Vib. **145**, 279 (1991).
[18]W. Chin, E. Ott, H. E. Nusse, and C. Grebogi, Phys. Rev. E **50**, 4427 (1994).
[19]Y. Yue and J. H. Xie, Int. J. Bifurcation Chaos **5**, 1250109 (2012).
[20]Y. Yue and J. H. Xie, Phys. Lett. A **373**, 2041 (2009).
[21]J. F. Mason and P. T. Piiroinen, Chaos **21**, 013113 (2011).
[22]J. F. Mason and P. T. Piiroinen, Chaos **22**, 013106 (2012).
[23]J.-P. Eckmann and D. Ruelle, Rev. Mod. Phys. **57**, 617 (1985).
[24]T. S. Parker and L. O. Chua, *Practical Numerical Algorithms for Chaotic Systems* (Springer-Verlag, 1989).
[25]S. Dawson, C. Grebogi, T. Sauer, and J. A. Yorke, Phys. Rev. Lett. **73**, 1927 (1994).
[26]H. E. Nusse and J. A. Yorke, Physica D **36**, 137 (1989).